

# A Radius of Robust Feasibility Approach to Directional Sensors in Uncertain Terrain

Vanshika Datta<sup>a</sup>, C. Nahak<sup>a</sup>

<sup>a</sup>*Department of Mathematics, Indian Institute of Technology Kharagpur, Kharagpur, West Bengal, India-721302*

## Abstract

A sensor has the ability to probe its surroundings. However, uncertainties in its exact location can significantly compromise its sensing performance. The radius of robust feasibility defines the maximum range within which robust feasibility is ensured. This work introduces a novel approach integrating it with the directional sensor networks to enhance coverage using a distributed greedy algorithm. In particular, we provide an exact formula for the radius of robust feasibility of sensors in a directional sensor network. The proposed model strategically orients the sensors in regions with high coverage potential, accounting for robustness in the face of uncertainty. We analyze the algorithm's adaptability in dynamic environments, demonstrating its ability to enhance efficiency and robustness. Experimental results validate its efficacy in maximizing coverage and optimizing sensor orientations, highlighting its practical advantages for real-world scenarios.

**Keywords:** Radius of robust feasibility; Voronoi diagram; Directional sensor network; Data uncertainty

**MSC:** 49K99; 65K10; 90C29; 90C46; 90C34

## 1. Introduction

Uncertainty, arising from prediction errors, measurement inaccuracies, implementation challenges and environmental variability, is a fundamental challenge in real-world scenarios. Traditional optimization models often assume perfect information, which is rarely available, leading to suboptimal or infeasible solutions [1, 5]. This highlights the need for methodologies that explicitly address data variability. Robust optimization (RO) meets this need by incorporating uncertainty directly into mathematical models through deterministic sets rather than probabilistic distributions. This approach offers a practical, flexible and risk-averse alternative to stochastic methods, particularly valuable when probabilistic data is unavailable or unreliable and in high-stakes, one-time decision-making scenarios.

The foundational idea of RO emerged with Soyster's 1973 work [25], which introduced a linear framework ensuring feasibility for all data within a convex uncertainty set. This initiated a systematic approach to handling uncertainty in optimization. The field gained significant traction in the late 1990s with the pioneering contributions of Ben-Tal, Nemirovski and El Ghaoui [4, 5, 6], who developed computationally tractable methods for both linear and nonlinear optimization problems under uncertainty. Over the years, RO has evolved into a powerful approach for risk-averse decision-making, extending from convex programs to robust discrete optimization [18], robust mixed-integer and nonlinear formulations [2, 21, 28, 30] and applications in robust linear programming [3], semidefinite programming [12] and conic-quadratic problems [7]. Survey studies [11, 19] confirmed RO's growing impact across operations research, engineering and finance, with recent advancements expanding into nonconvex and mixed-integer nonlinear programming [23], broadening its relevance to complex real-world scenarios.

RO addresses uncertainty by ensuring that solutions remain feasible for all parameter values within a predefined uncertainty set. While it effectively handles uncertain coefficients, a key challenge is ensuring the existence of robust feasible solutions under uncertain constraints. This highlights the importance of the radius of robust feasibility (RRF), which quantifies the maximum tolerable uncertainty while preserving feasibility. Initially defined for linear semi-infinite programming (LSIP) by Goberna et al. [14, 17], it has since been extended to

\*Corresponding author

Email address: cnahak@maths.iitkgp.ac.in (C. Nahak)

general linear and convex programs [10, 15]. Though early work focused on ball uncertainty sets, recent studies have generalized RRF to structures like spectrahedra. Chen et al. [9] analyzed RRF for uncertain convex inequalities with multi-convex, compact sets, deriving bounds, exact formulas under symmetry and tractable cases for ellipsoids, polytopes, boxes and the unit ball. Li and Wang [20] further provided an exact RRF formula and positivity conditions for general convex programs.

The concept of the RRF has been extended to uncertain mixed-integer linear programming, robust convex optimization and facility location design. A comprehensive survey by Goberna et al. [16] explored its role in continuous and mixed-integer robust optimization, emphasizing applications in logistics, network design and control systems. Their work offered a profuse collection of important references for further study. Computational approaches for RRF varied by problem structure: Goberna et al. [13] used semidefinite programming for linear and convex polynomial programs, while Boyd et al. [8] employed fractional programming and binary search for linear and mixed-integer cases.

Wireless and directional sensor networks (WSNs and DSNs) have emerged as vital tools for monitoring and tracking, yet their performance is often hindered by positional uncertainties. This issue is particularly pronounced in DSNs, which employ limited-angle sensors like cameras and lidar, making deployment strategies, sensor orientation and coverage optimization critical. In complex environments such as forests and disaster zones, deployment errors and environmental variability can degrade sensing performance, energy efficiency and communication reliability. While energy-efficient designs have been explored, uncertainty-resilient deployment remains under-addressed. The RRF offers a deterministic, structured framework to mitigate small positioning errors, enhancing robustness and sustainability in DSN operations. RRF has also found relevance in real-world domains such as supply chain management, gas network control [14], flexibility index problems [20] and facility location design [29], where uncertainty significantly impacts system performance. A. B. Ridolfi [22] significantly advanced this concept by shifting the focus from uncertain coefficients to location uncertainty, offering new perspectives in location-based optimization.

Inspired by A. B. Ridolfi's paradigm shift [10], we propose a novel RRF definition for DSNs, capturing robustness via an associated linear program. Our model integrates RO with a Voronoi-based distributed greedy algorithm that adaptively adjusts sensor orientations to maintain coverage under uncertainty. Simulations evaluate the effects of sensor count, viewing angles and sensing radii on coverage performance. We also introduce an iterative optimization strategy that refines sensor orientations to enhance adaptability. Although robust optimization has addressed distance uncertainty in WSNs [27], its application to DSNs under location uncertainty remains largely unexplored. Our work fills this gap by applying a robust continuous optimization framework to model DSN coverage with uncertain sensor locations. This avoids probabilistic assumptions, introduces an RRF based on location uncertainty, and ensures resilient, high coverage deployment through a distributed, orientation-aware approach.

The remainder of the article is structured as follows: Section 2 presents the necessary preliminaries, including the RRF, Voronoi region construction, the sensing model and problem description. Section 3 focuses on the RRF for DSNs, forming the basis of our robust optimization approach. Section 4 outlines the proposed model, detailing its design and objectives. Section 5 describes the methodology, encompassing the algorithmic framework and implementation. Section 6 provides an in-depth experimental analysis to validate the model under various configurations. Section 7 concludes with future directions.

## 2. Preliminaries

We begin by introducing some common notations, definitions and results. Let  $\mathbb{R}^n$  denote the Euclidean space,  $\|\cdot\|$  the Euclidean norm and  $\mathbb{B}_n$  the open unit ball in  $\mathbb{R}^n$ . We denote the transpose of a vector  $a$  by  $a^T$ . For  $x, y \in \mathbb{R}^n$ , the Euclidean distance is  $d(x, y) = \|x - y\|$ . Let  $S \subset \mathbb{R}^n$ , later referred to as the set of sensors, be a set with at least two elements and a fixed element  $s \in S$ . We denote its closure, convex hull and conical hull by  $cl(S)$ ,  $conv(S)$  and  $cone(S)$ , respectively. For a convex set  $S$ ,  $rint(S)$  and  $dim(S)$  denotes its relative interior and dimension. Furthermore,  $\mathbb{R}_+^S$  denotes set of functions  $r : S \rightarrow \mathbb{R}_+$ , while  $\mathbb{R}_+^{(S)}$  denotes subset of functions  $\lambda : S \rightarrow \mathbb{R}_+$  with nonzero values for only finitely many  $s \in S$ .

**Lemma 2.1.** (Schur complement[[6], Lemma 4.2.1])  $W := \begin{bmatrix} A & B^T \\ B & C \end{bmatrix}$  be a symmetric matrix with a positive definite matrix  $A$  of order  $k$  and block  $C$  of order  $l$ . Then,  $W$  is positive semi-definite if and only if  $C - BA^{-1}B^T$  is positive semi-definite.  $\blacksquare$

**Definition 2.1.** (Reference cone) Given a linear system  $\sigma := \{a_s^T x \leq b_s, s \in S\}$ , its reference cone  $K$  is defined as:

$$K := \text{clcone} \left\{ \begin{bmatrix} a_s \\ b_s \end{bmatrix}, s \in S; \begin{bmatrix} 0_n \\ 1 \end{bmatrix} \right\}.$$

Also, note that  $\sigma$  is consistent, [17], if and only if this reference vector does not belong to  $K$ , i.e.,  $\begin{bmatrix} 0_n \\ -1 \end{bmatrix} \notin K$ .

The system  $\sigma$  is called continuous if  $S$  is compact and the functions  $a : S \rightarrow \mathbb{R}^n$ ,  $a(s) = a_s$  and  $b : S \rightarrow \mathbb{R}$ ,  $b(s) = b_s$ , are continuous.

A parametric linear system in the face of data uncertainty in its constraints, denoted by  $\sigma^\alpha$ , can be captured as follows:

$$\sigma^\alpha := \{a_s^T x \leq b_s, s \in S\}; (a_i, b_i) \in \mathbb{U}_i^\alpha \subset \mathbb{R}^{n+1}; i = 1 : p,$$

where  $(a_i, b_i)$  for  $i = 1 : p$  are uncertain vectors and  $\mathbb{U}_i^\alpha$ ;  $i = 1 : p$ , which are typically assumed to be compact and convex.

The robust counterpart (deterministic form) of the corresponding system  $\sigma^\alpha$  with  $U_i^\alpha = (\bar{a}_s, \bar{b}_s) + \alpha B_{n+1}$ ,  $s \in S$ ,  $i = 1 : p$  and the corresponding feasible set  $F_R^\alpha$  for some  $\alpha \in \mathbb{R}$  is:

$$\sigma_R^\alpha := \{a_s^T x \leq b_s, \forall (a_s, b_s) \in U_i^\alpha, s \in S\}.$$

## 2.1. Construction of Voronoi Regions

A Voronoi diagram is a spatial decomposition of a region based on proximity to a given set of points, called generators (sensor nodes in our case).

**Definition 2.2.** (Voronoi cell) Given a set of generator points  $S = \{s_1, s_2, \dots, s_n\}$  in  $\mathbb{R}^2$ , the Voronoi cell  $V_S(s_i)$  associated with sensor  $s_i \in S$  is defined as:

$$V_S(s_i) = \{p \in \mathbb{R}^2 : d(p, s_i) \leq d(p, s_j) \text{ for all } j \neq i\},$$

where  $j = 1 : n$ ,  $d(a, b)$  is the Euclidean distance between  $a$  and  $b$ .

The Voronoi diagram consists of the union of all Voronoi cells (see Figure 1).

## 2.2. Radius of Robust Feasibility

The radius of robust feasibility ( $\rho$ ) of an uncertain system ( $\sigma^\alpha$ ) determines the maximum level of perturbation that a system can tolerate while remaining feasible. It is formally defined as follows:

**Definition 2.3.** (Radius of robust feasibility) Consider a parametric linear system in face of data uncertainty  $\sigma^\alpha$ . Let  $F_R^\alpha$  denote the feasible set of the robust counterpart of  $\sigma^\alpha$ . Then, the RRF for the system is given by:

$$\rho = \sup\{\alpha \in \mathbb{R}_+ : (F_R^\alpha) \text{ is nonempty}\}.$$

This quantifies the maximum perturbation level under which the system remains robustly feasible. A fundamental concept in computing RRF is the Minkowski function, defined as follows:

**Definition 2.4.** (Minkowski function) Let  $\omega \subset \mathbb{R}^n$  be a convex set containing  $0_n$  in its interior. Then the Minkowski or gauge function of  $\omega$  denoted by  $\phi_\omega$ , where  $\phi_\omega : \mathbb{R}^n \rightarrow \mathbb{R}_+ := [0, +\infty[$  is given by:

$$\phi_\omega(x) := \inf \{t > 0 : x \in t\omega\}, x \in \mathbb{R}^n.$$

The following lemma provides some properties of the Minkowski function.

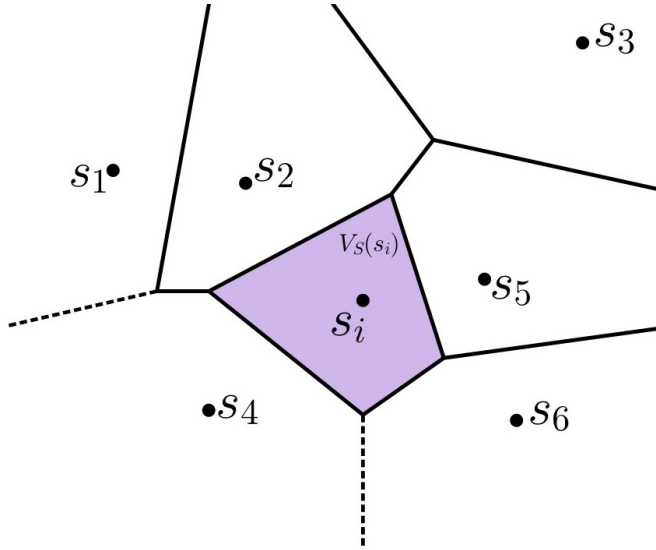


Figure 1: Voronoi diagram for a set of sensors  $s_1, s_2, s_3, s_4, s_5, s_6, s_i$

**Lemma 2.2** ([24], Lemma 1.3.13). *Let  $\omega \subset \mathbb{R}^n$  be a convex set such that its interior contain  $0_n$ , then, the following properties hold:*

- (1)  $\phi_\omega$  is sublinear and continuous.
- (2)  $\{x \in \mathbb{R}^n : \phi_\omega(x) \leq 1\} = \text{cl}(\omega)$ , where  $\text{cl}(\omega)$  stands for the closure of  $\omega$ .
- (3) If in addition,  $\omega$  is bounded and symmetric, then,  $\phi_\omega := \|\cdot\|$  is a norm on  $\mathbb{R}^n$  generated by  $\omega$ . ■

The next lemma defines a dual characterization of solutions of a semi-infinite linear inequality system, which is useful for our analysis in the sequel. It is found in [17].

**Lemma 2.3.** *Let  $I$  be an arbitrary index set. Then,*

$$\{x \in \mathbb{R}^n : a_i^T x \leq b_i : i \in I\} \neq \emptyset \iff (0_n, 1) \notin \text{clcone} \{(-a_i, -b_i) : i \in I\}. \quad \blacksquare$$

The next lemma is an extension of [13], which uses the epigraphs of conjugate functions of convex functions.

**Lemma 2.4.** *Let  $\alpha \in \mathbb{R}_+$  and  $(a_i, b_i) \in \mathbb{R}^{n+1}$ ;  $i = 1 : p$ . Also let  $\mathbb{U}_i^n$  be the set defined in the beginning of this section. If*

$$(0_n, 1) \in \text{clcone} \{\cup_{i=1}^p [(-\bar{a}_i, -\bar{b}_i) - \alpha \mathbb{U}_i^n]\}$$

*holds, then for all  $\delta > 0$ , we have*

$$(0_n, 1) \in \text{cone} \{\cup_{i=1}^p [(-\bar{a}_i, -\bar{b}_i) - (\alpha + \delta) \mathbb{U}_i^n]\}.$$

Exact formula of RRF for an arbitrary set  $S$  has been obtained in literature in terms of the so-called hypographical set  $H(\bar{a}, \bar{b})$  of the nominal system  $\sigma$ :

$$H(\bar{a}, \bar{b}) := \text{conv} \{(-\bar{a}_i, -\bar{b}_i) : i = 1 : p\} + \mathbb{R}_+(0_n, -1),$$

where  $\bar{a} = (\bar{a}_1, \bar{a}_2, \dots, \bar{a}_p) \in (\mathbb{R}^n)^p$  and  $\bar{b} = (\bar{b}_1, \bar{b}_2, \dots, \bar{b}_p) \in \mathbb{R}^p$ .

**Theorem 2.1.** [10] *If the nominal system is feasible, the RRF of  $\sigma^\alpha$  is:*

$$\rho = \inf_{(a,b) \in H(\bar{a}, \bar{b})} \phi_Z(a, b),$$

where  $Z \subset \mathbb{R}^n$  is a convex and compact set containing  $0_n$  in its interior.

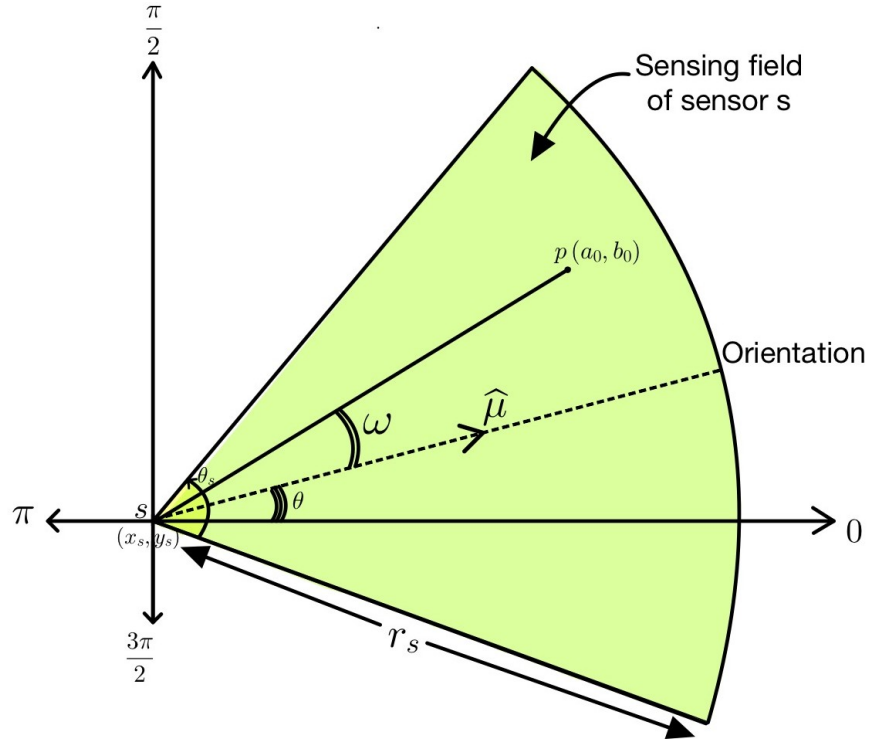


Figure 2: Sensing model for directional sensors

### 2.3. Sensing Model in Directional Sensor Networks

In directional sensor networks (DSNs), each sensor has a limited sensing angle and range, as shown in Figure 2. Here,  $r_s$  is the sensing range of the sensor  $s$ , located at  $(x_s, y_s)$ .  $\hat{\mu}$  is a unit vector denoting the orientation of the sensor. Note that each sensor has only one orientation  $\mu$ , making an angle  $\theta$  lying between  $-\pi$  and  $\pi$  relative to the positive  $x$  direction. The effective sensing field, called the field of view of the sensor, is a sector denoted by the shaded part in the figure. It is formed using two side lengths of sensing sector with radius  $r_s$  and an included angle  $\theta_s$ , which is the angle of view or effective viewing angle.

Note that the sensor ‘ $s$ ’ positioned at  $(x_s, y_s)$  with sensing range  $r_s$  and sensing angle  $\theta_s$  covers a point  $p(a_0, b_0)$  if the following two conditions are satisfied:

- (1) The Euclidean distance between point  $p$  and sensor  $s$  is less than or equal to the sensing radius  $r_s$  of sensor ‘ $s$ ’, i.e.,

$$\sqrt{(x_s - a_0)^2 + (y_s - b_0)^2} \leq r_s.$$

- (2) The included angle  $\omega$  between  $\vec{sp}$  and  $\hat{\mu}$  is less than or equal to half of the angle of view  $\theta_s$  of sensor ‘ $s$ ’, i.e.,

$$\omega \leq \frac{\theta_s}{2}.$$

### 2.4. Problem Description

We address the issue of uncertainty in the sensor locations. Traditional placement models either ignore uncertainty or rely on known probabilistic distributions, which are not always available. Our approach considers the robustness of maximizing the coverage by incorporating the RRF. The main goals are:

- (1) Introducing the concept of RRF for directional sensor networks.
- (2) Maximizing the coverage while ensuring robust feasibility under worst location of sensor nodes using the concept of RRF of directional sensor networks.
- (3) Improve deployment adaptability through an iterative RO approach.

We use a distributed greedy algorithm that iteratively refines sensor orientation while accounting for uncertainty, ensuring optimal coverage with minimal resource usage.

### 3. Radius of Robust Feasibility for Directional Sensor Networks

In this section, inspired by Chuong et al. and Sung et al. [10, 26], we extend the RRF concept to Voronoi cells with sensor-induced coefficient uncertainty. We provide a distinct definition of RRF for the DSNs in the case of ball uncertainty. We consider a set of directional sensors  $S \subset \mathbb{R}^2$ , each subject to location uncertainty. In fact, we allow only perturbations on the coefficients of the system  $\sigma$  defined in Definition 2.1, which comes from the uncertainty of sensor nodes  $s \in S$ . Hence, instead of considering arbitrary perturbations in the coefficients  $(a_s, b_s)$  in  $\sigma^\alpha$ , we consider only those changes that result from the sensor locations being unknown and therefore subject to perturbations due to uncertainty. In this way, we set up the following notation.

For a particular sensor  $s_i \in S = \{s_1, s_2, \dots, s_n\}$ , let the nominal location be  $\bar{s}_i$  and let the uncertainty set be  $\mathbb{U}_i^\alpha$ ;  $i = 1 : n$ , defined by:

$$\mathbb{U}_i^\alpha := \bar{s}_i + \alpha \mathbb{B}_2; \quad i = 1 : n,$$

where  $\mathbb{B}_2$  denotes the closed unit ball in  $\mathbb{R}^2$ , which is convex and compact with  $0_2 \in \text{int}(\mathbb{B}_2)$ . This structured formulation allows the derivation of robustness conditions that are physically grounded in sensor placement errors. Assuming the nominal system  $\sigma$  is feasible, we now define the worst-case sensor position ‘ $s_o$ ’ for sensor  $s_i \in S$  along the direction of sensing  $\vec{u}$ , which gives a meaningful and tractable representation for robust coverage analysis:

$$s_o = \bar{s}_i + \alpha \frac{\vec{u}}{|\vec{u}|}.$$

Then, for a fixed realization  $s_i = (\bar{x}_i, \bar{y}_i) \in S$ , the Voronoi cell  $VC(s_i)$ , by Definition 2.2, corresponds to the system of inequalities:

$$VC(s_i) := \{x \in \mathbb{R}^2 : \|x - s_i\|_2^2 \leq \|x - s_j\|_2^2, \forall j \neq i\}.$$

Expanding the norms and rearranging terms, the inequality becomes

$$VC(s_i) = \{x \in \mathbb{R}^2 : 2(s_j - s_i)^T x \leq \|s_j\|_2^2 - \|s_i\|_2^2, \forall j \neq i\},$$

which defines the half-space constraints forming the Voronoi cell of  $s_i$ . We aim to express the induced uncertainty in the coefficients  $(a_{ij}, b_{ij})$  due to the uncertainty in  $s_i$ . Let us define:

$$a_{ij} := 2(s_j - s_i) \in \mathbb{R}^2 \text{ and } b_{ij} := \|s_j\|_2^2 - \|s_i\|_2^2 \in \mathbb{R}. \quad (3.1)$$

Then  $a_{ij}^T x \leq b_{ij}$  becomes the Voronoi half-space system of constraints under uncertainty. This leads to an uncertainty set in the coefficients  $(a_{ij}, b_{ij})$ , which are functions of  $(s_i, s_j)$ . Next, we consider the set of all such uncertain locations of  $s$  which are contained in the Voronoi cell of  $s_i$ . Note that the feasible set of such balls is the same as the following feasible set:

$$\mathcal{F}^\alpha = \{x \in \mathbb{R}^2 : a_{ij}(s_i, s_j)^T x \leq b_{ij}(s_i, s_j), \forall j \neq i, \forall s_i \in \mathbb{U}_i^\alpha, \forall s_j \in \mathbb{U}_j^\alpha\}. \quad (3.2)$$

Define the uncertainty set for the coefficients as:

$$\begin{aligned} \mathbb{U}_{ij}^\alpha &:= \{(a_{ij}, b_{ij}) \in \mathbb{R}^3 : s_i \in \bar{s}_i + \alpha \mathbb{B}_2, a_{ij} := 2(s_j - s_i) \in \mathbb{R}^2, \\ &\quad b_{ij} := \|s_j\|_2^2 - \|s_i\|_2^2, \forall s_i \in \mathbb{U}_i^\alpha, \forall s_j \in \mathbb{U}_j^\alpha\}. \end{aligned} \quad (3.3)$$

This defines a nonlinear uncertainty set in  $(a, b)$ , induced from the ball uncertainty in  $s_i$ . The nonlinear uncertainty set in  $(a, b)$  must be approximated linearly for tractability and compatibility with robust optimization frameworks. Hence, to align our model with the linear uncertainty framework in the literature, we use the Taylor expansions to approximate the nonlinear functions of  $s_i$  and  $s_j$  that define  $a_{ij}$  and  $b_{ij}$ , thereby obtaining linear expressions that can be used to define linear uncertainty sets. To this end, we assume  $s_i = \bar{s}_i + \Delta s_i$  and

$s_j = \bar{s}_j + \Delta s_j$ , with  $\|\Delta s_i\|, \|\Delta s_j\| \leq \alpha$ . Also, let us define using equation (3.1) that  $a = 2(s_j - s_i)$  and  $b = \|s_j\|^2 - \|s_i\|^2$  have their nominal values as:  $\bar{a} = 2(\bar{s}_j - \bar{s}_i)$  and  $\bar{b} = \|\bar{s}_j\|^2 - \|\bar{s}_i\|^2$ . Hence, we have

$$a = \bar{a} + 2(\Delta s_j - \Delta s_i).$$

Rearranging this, we get

$$\|a - \bar{a}\| \leq 2(\|\Delta s_j\| + \|\Delta s_i\|) \leq 4\alpha.$$

Similarly, we have:  $b = \|s_j\|^2 - \|s_i\|^2$ , we use the first-order Taylor expansions

$$\|s_j\|^2 \approx \|\bar{s}_j\|^2 + 2\bar{s}_j^T \Delta s_j,$$

and

$$\|s_i\|^2 \approx \|\bar{s}_i\|^2 + 2\bar{s}_i^T \Delta s_i.$$

This implies that

$$b \approx \bar{b} + 2(\bar{s}_j^T \Delta s_j - \bar{s}_i^T \Delta s_i).$$

Now, we bound the deviation from  $\bar{b}$ :

$$\begin{aligned} \|b - \bar{b}\| &\leq 2(\|\bar{s}_j^T \Delta s_j\| + \|\bar{s}_i^T \Delta s_i\|) \\ &\leq 2(\|\bar{s}_j\| \cdot \|\Delta s_j\| + \|\bar{s}_i\| \cdot \|\Delta s_i\|) \\ &\leq 2\alpha(\|\bar{s}_j\| + \|\bar{s}_i\|) \\ &:= \delta_b(\alpha). \end{aligned}$$

Now, we define the linear uncertainty set for a particular  $i \in \{1, 2, \dots, n\}$  using equation (3.3) as follows:

$$\mathbb{U}_i = \{(a, b) : \|a - \bar{a}\| \leq 4\alpha, \|b - \bar{b}\| \leq \delta_b(\alpha)\}, \forall j = 1 : n, j \neq i. \quad (3.4)$$

Hence, our robust feasible region from equation (3.2) and equation (3.4) becomes

$$\mathcal{F}^\alpha = \{x \in \mathbb{R}^2 | a^T x \leq b, \forall (a, b) \in \mathbb{U}_i \ \forall j \neq i\},$$

yielding a standard tractable uncertainty model, compatible with robust optimization and we can compute the RRF for this using similar approach as in [10]. Hence, we define the robust feasible region for sensor  $s_i \in S$  as the intersection of these uncertain half-spaces. We now define the notion of RRF for DSN as follows:

**Definition 3.1.** (Radius of robust feasibility for DSN) Let  $S$  be a set of sensors in a DSN. The radius of robust feasibility for directional sensor  $s_i$  is the largest uncertainty radius  $\alpha$  such that its robust feasible region  $\mathcal{F}^\alpha$  remains nonempty for a sensor  $s_i \in S$ , i.e.,

$$\rho_s = \sup \{\alpha \in \mathbb{R} \geq 0 : \mathcal{F}^\alpha \neq \emptyset \ \forall i = 1 : n\}.$$

The RRF  $\rho_s$  defines the largest uncertainty radius ensuring feasibility. In sensor networks, it accounts for minor displacements from nominal positions and guides the maximum permissible deviation when exact deployment is infeasible.

Hence, we state the first main result of the paper in the following theorem, which gives an exact formula for the RRF of a sensor in a directional sensor network.

**Theorem 3.1.** (Exact RRF formula) Let the nominal system  $\sigma$  be feasible. Then, the RRF of a sensor ‘ $s$ ’ in a directional sensor network is:

$$\rho = \inf_{x \in \mathcal{F}^\alpha} \min_i \frac{\bar{b}_i - \bar{a}_i^T x}{\xi_{\mathbf{Z}_i}(x, -1)},$$

where  $\xi_{\mathbf{Z}_i}(x, -1)$  is the support function of the uncertainty set  $\mathbf{Z}_i$ , capturing worst-case directional perturbation.

*Proof* We begin with the definition of RRF for a system with uncertain linear constraints:

$$(a_i, b_i) \in (\bar{a}_i, \bar{b}_i) + \rho \mathbf{Z}_i \quad i = 1 : n.$$

We want the system to remain feasible under all such perturbations, i.e., to find  $\rho$  such that

$$\bigcap_{(a_i, b_i) \in (\bar{a}_i, \bar{b}_i) + \rho \mathbf{Z}_i} \{x \mid a_i^T x \leq b_i\} \neq \emptyset.$$

This is the same as

$$\forall i, \sup_{(a_i, b_i) \in (\bar{a}_i, \bar{b}_i) + \rho \mathbf{Z}_i} (a_i^T x - b_i) = \rho \cdot \xi_{\mathbf{Z}_i}(x, -1) \leq \bar{a}_i^T x - \bar{b}_i,$$

where  $\xi_{\mathbf{Z}_i}(x, -1)$  denotes the support function of the uncertainty set  $\mathbf{Z}_i$ , evaluated in the direction  $(x, -1)$ . We get

$$\rho \leq \frac{\bar{b}_i - \bar{a}_i^T x}{\xi_{\mathbf{Z}_i}(x, -1)}.$$

To ensure all constraints remain satisfied under uncertainty, we take the minimum over all  $i$  and then to get the maximum feasible radius, we take the infimum over all feasible  $x \in \mathcal{F}^\alpha$ . As a result, we get

$$\rho = \inf_{x \in \mathcal{F}^\alpha} \min_i \frac{\bar{b}_i - \bar{a}_i^T x}{\xi_{\mathbf{Z}_i}(x, -1)},$$

which is the required expression, thereby concluding the proof. ■

Note that the expression in Theorem 3.1 quantifies the robustness margin  $\rho$  for the sensor  $s_i$  by minimizing over positions  $x$  within its nominal Voronoi cell while accounting for the worst-case deviation in each constraint. The formula enables tractable computation of robust Voronoi regions even under spatial uncertainty. Next, we state the following theorem, which will be helpful in our application of directional sensor network area coverage for selecting the working direction of a particular sensor.

**Theorem 3.2.** *The working direction of a sensor to maximize the coverage is towards a vertex in the Voronoi diagram.*

*Proof* Consider a Voronoi diagram  $V(S)$  generated by a finite set of sensor locations  $S$  in a Euclidean plane. Each Voronoi cell is a convex polygon whose vertices are equidistant from at least three sensors.

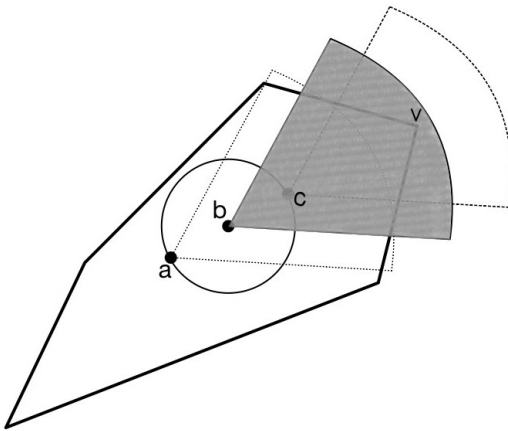
Let us assume, if possible, there exists a point  $P$  in a Voronoi cell that is farther from its associated sensor than any vertex of the cell. Since  $P$  is not a vertex and is farther than a vertex, it must lie on the edge of the Voronoi cell. However, this assumption leads to a contradiction based on the following reasoning:

- (1) Due to the convexity of the Voronoi cell, any infinitesimal displacement of  $P$  along the edge, either left or right, remains within the cell. Consequently, no such perturbed point can exceed  $P$  in distance from the sensor, contradicting the assumption that  $P$  is the farthest point.
- (2) If both adjacent points to  $P$  on an edge are equidistant from the sensor, the edge would form a circular arc centered at the sensor. However, Voronoi edges in a Euclidean diagram with finitely many sensors are always straight-line segments, leading to a contradiction—thus, such a point  $P$  cannot exist.

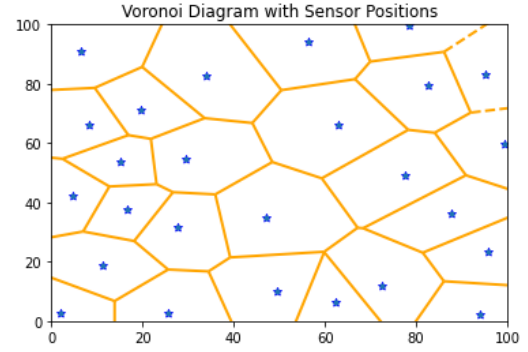
Thus, the farthest point within a Voronoi cell must always be at a vertex, proving that the optimal working direction of a sensor is towards a vertex. ■

#### 4. Proposed Model

A key challenge in DSNs is determining an uncertainty-aware sensor field that reduces cost while providing high coverage. Using RRF for DSN orientation adjustments enables sensors to cover more area with fewer gaps caused by minor positional shifts, which is especially useful in unpredictable environments. We begin by describing our sensing model, then formulate the corresponding optimization problem, outline the key constraints and conclude with a discussion of the main assumptions and structural properties of the problem.



(a) Best and worst-case coverage of a sensor



(b) Construction of Voronoi diagram

Figure 3: Illustration of sensor coverage analysis

#### 4.1. Sensing Model and Problem Definition

Sensor placement often deviates from nominal locations due to obstacles like water bodies or deployment errors, especially in randomly deployed networks where precise positioning is impractical. We address this by formulating an approach to compute the maximum allowable uncertainty radius around each nominal position that ensures robust feasibility. An iterative algorithm is then used to determine this radius and orient each sensor optimally to maximize coverage under positional uncertainty. Our model primarily consists of a directional sensor network, where each sensor has specific coverage areas defined by its orientation and effective range. For a particular sensor ‘s’, the effective coverage area is given by

$$A_s = \theta_s \cdot r_s^2,$$

where  $\theta_s$  is the angle of coverage in radians and  $r_s$  is the effective coverage range. However, we will need the intersection of this coverage area with the Voronoi region of ‘s’.

Figure 3a illustrates the best- and worst-case sensor placement scenarios when facing a vertex ‘v’. The uncertainty in sensor positioning is represented by a circular region centered at its nominal location ‘b’, within which the sensor may be positioned. This variability affects the effective coverage area. To ensure robust performance under the worst-case uncertainty, we assume the most disadvantageous sensor placement while determining its optimal orientation. The shaded region denotes the nominal area it covers; the bounded dotted and dashed regions denote the area it covers under the best and worst-case, respectively. Thus, the sensor is considered to be at location ‘c’, where its coverage within its Voronoi cell is minimized. If the optimal orientation aligns towards vertex ‘v’, the guaranteed coverage will be at least that achieved when the sensor is positioned at ‘c’, while in the best-case scenario, it could be maximized if the sensor is located at ‘a’.

**Example 4.1** (Single sensor with positional shift). *Let a sensor ‘s’ have a coverage range of  $s_r = 100$  m and a positional uncertainty of  $\rho_s = 5$  m. The robust coverage range is then given by  $r_s = s_r - \rho_s$ , resulting in 95 m. Since this represents the worst-case scenario, the sensor can ensure coverage of at least 95 m within its Voronoi cell when oriented toward the specified vertex.*

#### 4.2. Optimization Formulation

From now on, we restrict our attention to a bounded region  $R$  and  $m$  sensors. Given a set  $S$  of  $m$  directional sensors  $s_1, s_2, \dots, s_m$  in a two-dimensional sensing field, a Voronoi diagram (see Figure 3b) is constructed by drawing the perpendicular bisectors of the line segments connecting each pair of sensors. These bisectors form the boundaries of Voronoi cells, known as Voronoi edges, while their intersection points are referred to as Voronoi vertices. As a result, the field is partitioned into ‘ $m$ ’ Voronoi cells with the following characteristics:

- (1) Each sensor  $s_j$  is contained within a unique cell.

- (2) Any point ‘ $p$ ’ inside the Voronoi cell of the sensor  $s_j$  is closer to the sensor  $s_j$  than any other sensor  $s_t$  for all  $j, t \in \{1, 2, \dots, m\}, j \neq t$ .
- (3) The Voronoi diagram for a given set of sensors is uniquely determined, meaning that the same set of points will always generate the same Voronoi structure.

Based on the characteristics of a Voronoi cell, the sensor within a given cell has the strongest inductive capacity or the best sensing quality for any position inside that cell. Therefore, each sensor should be responsible for covering its respective cells as fully as possible. Additionally, since Voronoi cells are always convex polygons, Theorem 3.2 states that the farthest point within a cell from its associated sensor is typically one of the cell’s vertices.

Since we focus on perturbations caused by sensor location uncertainty rather than arbitrary system coefficient changes, we consider only variations arising when the sensor positions  $s_j \in S ; j = 1 : m$  are unknown and subject to uncertainty. Thus, we introduce the following notations.

Let  $I_j = \{1, 2, \dots, n_j\}$  represent the index set corresponding to sensor  $s_j$  for  $j = 1 : m$ , where  $n_j$  denotes the number of vertices in the Voronoi cell of  $s_j$ . The vertices of the Voronoi region associated with sensor  $s_j$  for  $i = 1 : n_j$  are denoted as  $v_{j_i}$ . The area covered by  $s_j$  within its Voronoi region when oriented towards vertex  $v_{j_i}$  is represented as  $A_{j_i}$ . Furthermore, let  $V_j$  and  $A_j$  denote the optimal orientation vertex selected and the corresponding covered area for sensor  $s_j$  within its Voronoi region, respectively, for  $j = 1 : m$ .

To maximize the total coverage while ensuring robustness against positional uncertainty, we formulate the following optimization problem:

$$\max \sum_{j=1}^m A_j,$$

subject to constraints ensuring that the sensor orientations account for worst-case positioning within the uncertainty set, thereby guaranteeing robust feasible coverage across the entire network. Hence, we have the following constraints:

- (1) **Initial Orientation Selection:** Each sensor selects the vertex that provides the maximum coverage within its Voronoi cell:

$$V_j = \arg \max_{v_{j_i} \in I_j} A_{j_i}, \quad \forall j \in \{1, 2, \dots, m\}.$$

- (2) **Overlap Resolution Constraint:** If two sensors select the same vertex, the sensor with the lower coverage area selects the next best option:

$$V'_j = \arg \max_{\substack{v_{j_i} \in I_j \\ v_{j_i} \neq V_j}} A_{j_i}, \quad \text{if } V_j = V_k \text{ and } A_j < A_k.$$

- (3) **Boundary Avoidance Constraint:** Sensors should not orient towards vertices that are within an  $\epsilon$ -distance of the boundary  $\partial R$ :

$$V_j \notin \{v_{j_i} \in I_j \mid d(v_{j_i}, \partial R) < \epsilon\}, \quad \forall j = 1 : m.$$

- (4) **Uncertainty Constraint:** Each sensor’s actual location  $(x_j, y_j)$  lies within an uncertainty ball of radius  $r_j$  around its nominal position  $b_j$ :

$$(x_j, y_j) \in B(b_j, r_j), \quad \forall j = 1 : m.$$

where  $(x_j, y_j)$  denotes the actual position of sensor  $s_j$ , constrained within its uncertainty set. This optimization model ensures that:

- (1) Sensors are oriented for maximum coverage within their Voronoi regions.
- (2) Overlapping orientations are resolved dynamically by reassigning the sensor with lower coverage.
- (3) Sensors avoid aligning towards vertices near the boundary for better stability.
- (4) The model accounts for uncertainty in sensor positioning, ensuring robust feasible coverage.

If a sensor  $s_j$  changes its orientation due to overlap resolution and all vertex options are exhausted, the sensor can either be put into sleep mode to conserve energy or select the initially preferred vertex. The following example shows that even if the sensor selects initially preferred vertex, it can still contribute to the robustness of the overall model.

**Example 4.2** (Overlapping Sensors with RRF Constraint). *Suppose sensors  $s_1$  and  $s_2$  are placed 150 m apart and both oriented toward the same vertex  $V$ , with robust ranges of  $r_{s_1} = 80$  m and  $r_{s_2} = 90$  m. This results in an overlapping coverage area, leading to unnecessary redundancy. To mitigate this, the sensor contributing lesser effective coverage within its Voronoi cell, say  $s_1$ , could be reoriented toward an alternative vertex. However, if all other vertices are already assigned to sensors with coverage greater than that of the selected sensor, then  $s_1$  may still remain oriented toward  $V$ , ensuring robustness against positional uncertainty. The overlap,  $\epsilon = 80 + 90 - 150 = 20$  m, acts as a buffer against deployment errors, preventing coverage gaps and maintaining reliable sensing.*

**Visual representation:** *Imagine two sectors representing the feasible regions of  $s_1$  and  $s_2$ , slightly overlapping. Even if  $s_1$  or  $s_2$  moves slightly within their feasible radii, the overlapping area remains covered, ensuring robust coverage continuity.*

A connectivity or energy constraint can also be incorporated into the constraint set; however, we omit it here as our focus is solely on maximizing coverage while accounting for location uncertainty. Additionally, a constraint ensuring that the covered area exceeds a threshold  $\epsilon$  could be introduced; otherwise, the sensor can be put into sleep mode to conserve energy.

### 4.3. Geometric Considerations and Assumptions

To streamline our analysis, we assume the region is bounded, with positional uncertainty modeled as a ball centered at each sensor's nominal location. Additionally, as discussed earlier, we focus exclusively on perturbations arising from uncertain sensor positions, rather than general coefficient variations.

In Figure 4, sensors exhibit different coverage patterns within their respective Voronoi cells. This leads to four distinct cases, illustrated in Figure 5, into which all other configurations can be categorized.

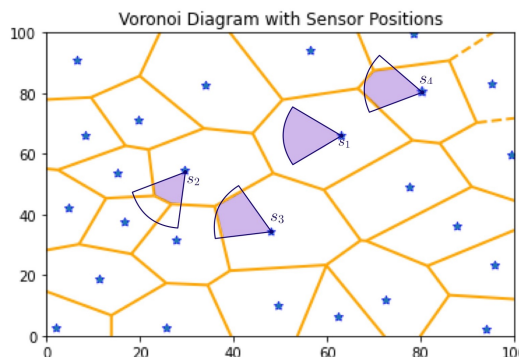


Figure 4: Possible cases for area coverage

#### 4.4. Stopping Condition and Practical Considerations

Since we aim to determine the worst-case scenario for real-world applications, we impose both upper and lower bounds on the RRF of each sensor. In practical settings, the RRF of a sensor is finite, as beyond a certain distance from the nominal location, the sensor is guaranteed not to be deployed. Therefore, we define a maximum RRF value,  $r_{max}$ , beyond which further extension is unnecessary. Similarly, since the RRF must be above a certain threshold in real-life environments, we establish a minimum allowable value,  $r_{min}$ . As a constraint, if the computed RRF of a sensor exceeds  $r_{max}$ , it is set to  $r_{max}$ ; if it falls below  $r_{min}$ , it is set to  $r_{min}$ . Hence, for each  $s_j$  where  $j = 1 : m$ , we have

$$r_{min} \leq \rho_s \leq r_{max}.$$

Additional refinements can be incorporated into the algorithm. For instance, a stopping criterion can be introduced where the algorithm terminates once a predefined coverage requirement is met. Another approach could involve ceasing the addition of new sensors when the incremental coverage gain from deploying an additional sensor falls below a threshold  $\delta$ , ensuring efficiency. Mathematically, this condition can be expressed as

$$A_2 - A_1 < \delta,$$

where  $A_1$  and  $A_2$  represent the coverage area before and after placing the new sensor, respectively. The parameter  $\delta$  regulates the trade-off between maximizing coverage and minimizing redundancy. However, such refinements are more relevant for structured deployment strategies rather than random sensor placement. Since our focus is on ensuring robust coverage under positional uncertainty, we do not incorporate these additional refinements in this study.

### 5. Proposed Methodology

Inspired by Sung et al. [26], this study utilizes Voronoi diagrams and direction-adjustable sensors to design an adaptive, distributed placement strategy that improves coverage in directional sensor networks. As outlined in Section 2.3, a point is covered if it satisfies two conditions, which, in the robust case, are evaluated using the sensor's robust location rather than nominal position. Consider the  $j^{th}$  sensor  $s_j$ ,  $j = 1 : m$ , be located at the nominal coordinates  $(x_j, y_j)$ , with an RRF  $\rho_j$ , and oriented toward vertex  $V = (a, b)$ . The direction vector from  $s_j$  to  $V$  is given by  $\vec{\mu} = (a - x_j, b - y_j)$ . After normalization and scaling by the RRF, the robust location of sensor  $s_j$  is given by  $t_j = (x'_j, y'_j)$  such that

$$\begin{aligned} (x'_j, y'_j) &= (x_j, y_j) + \rho_j \frac{\vec{\mu}}{|\vec{\mu}|} \\ &= (x_j, y_j) + \rho_j \left( \frac{a - x_j}{\sqrt{(a - x_j)^2 + (b - y_j)^2}}, \frac{b - y_j}{\sqrt{(a - x_j)^2 + (b - y_j)^2}} \right). \end{aligned} \quad (5.1)$$

Thus, a point  $p(a_0, b_0)$  is considered covered by sensor  $s_j$  if it meets the following conditions:  $d(t_j, p) \leq r_j$  and  $\omega \leq \frac{\theta_s}{2}$ , where  $r_j$  and  $\theta_s$  denote the effective robust coverage range and effective angular coverage range of sensor  $s_j$ , respectively. The parameter  $\omega$  represents the angle between the vector  $\vec{sp}$  and the unit vector  $\hat{\mu}$ .

Note that if  $\theta$  is the angle between  $\hat{\mu}$  and the relative positive x-axis with  $-\pi \leq \theta \leq \pi$ , one can derive the following from the second condition:

$$\begin{aligned} \vec{sp} \cdot \hat{\mu} &= \|\vec{sp}\| \|\hat{\mu}\| \cos \omega \\ \implies (a_0 - x'_j) \cos \theta + (b_0 - y'_j) \sin \theta &= \sqrt{(a_0 - x'_j)^2 + (b_0 - y'_j)^2} \cos \omega \\ \implies (a_0 - x'_j) \cos \theta + (b_0 - y'_j) \sin \theta &\geq \sqrt{(a_0 - x'_j)^2 + (b_0 - y'_j)^2} \cos \frac{\theta_s}{2}. \end{aligned} \quad (5.2)$$

Thus, a point  $p(a_0, b_0)$  is considered covered by sensor  $s_j$  under robust case if it satisfies inequalities  $d(t_j, p) \leq r_j$  and equation (5.2).

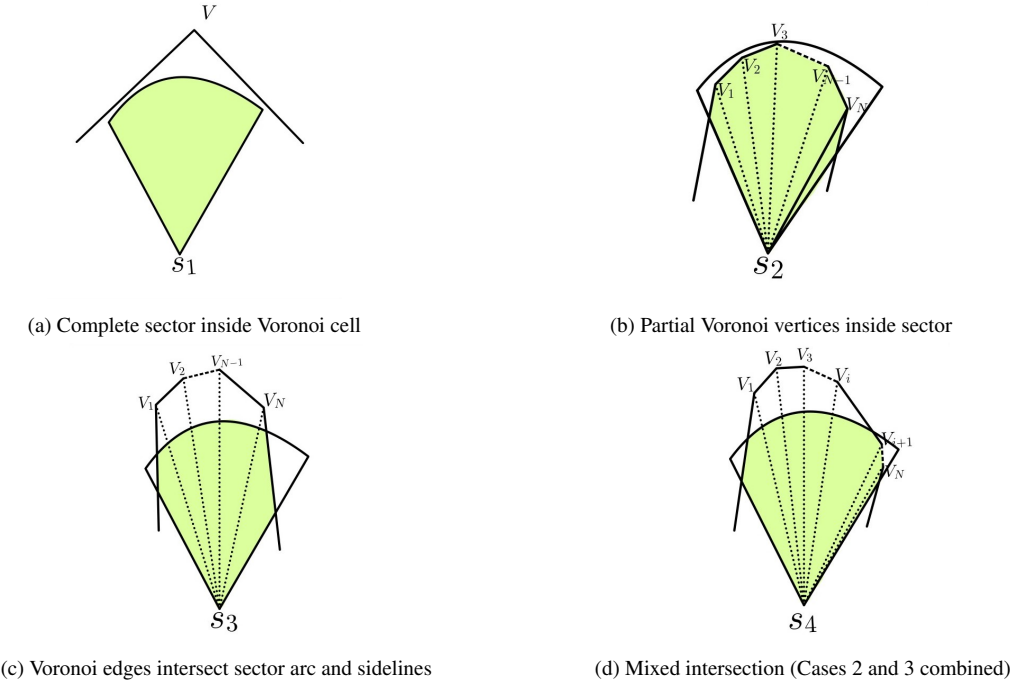


Figure 5: Illustration of the four possible cases of sensor coverage within a Voronoi cell

### 5.1. Greedy Sensor Placement Algorithm

Our approach iteratively refines sensor orientation and placement without requiring global information. The strategy follows three key principles. First, each sensor optimizes its orientation based on local Voronoi structures to maximize immediate coverage. Second, neighboring sensors collaboratively adjust their orientations to reduce coverage redundancy and fill sensing gaps. Finally, sensors near the boundary refine their orientations to prevent excessive coverage spillover and enhance the useful sensing area.

The process begins with the initialization of deployment, wherein the sensor field and parameters are defined, including the region  $R$ , the number of deployed sensors  $m$  and the angle of view  $\theta_s$  for all sensors. Based on the nominal placements, a Voronoi diagram is constructed to segment the sensing region.

Once the Voronoi diagram is established, the robust sensor locations are updated using Theorem 3.1 and equation (5.1) to account for positional uncertainty. After determining these robust locations, sensor orientations are optimized to maximize coverage by applying the localized sensor orientation optimization principle.

The algorithm then iterates through the update process, reconstructing the Voronoi diagram and refining sensor placements until either no two sensors are oriented towards the same vertex or all possible vertex reassignments for sensors with overlapping orientations have been exhausted.

### 5.2. Localized Orientation Optimization

Each sensor initially determines its orientation based on its Voronoi cell structure using a localized orientation approach. Since Voronoi vertices are equidistant from three or more sensors, they naturally serve as candidate directions (see Theorem 3.2). To align each sensor for maximum coverage, the coverage area corresponding to its robust location is computed for each candidate vertex and the orientation that yields the highest coverage is selected as the optimal direction. To compute this area, we focus on the sensor's coverage within its own Voronoi cell. This results in four possible interaction cases between the sensor and its cell, as seen for sensors  $s_1, s_2, s_3$  and  $s_4$  in Figure 4. We analyze each of these cases individually.

**Case-1: Complete sector inside Voronoi cell** [see  $s_1$  in Figure 5a]. If the entire sensing sector of a sensor  $s_j$  lies within its Voronoi cell, the coverage area  $A_j$  is simply given by the sector area formula:

$$A_j = \frac{\theta_s}{2} r_s^2,$$

where  $\theta_s$  is the sensor's field of view in radians and  $r_s$  is its effective coverage range.

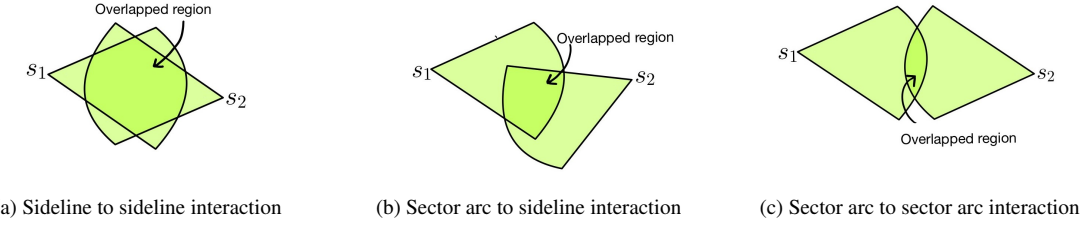


Figure 6: Possible interactions within different directional sensors

**Case-2: Partial Voronoi vertices inside sector** [see  $s_2$  in Figure 5b]. When some Voronoi vertices fall inside the sensing sector and two Voronoi edges intersect the sector's sidelines, the coverage area is computed by dividing the region into  $N + 1$  triangles formed by connecting the sensor location to each vertex. The area of each triangle is obtained using Heron's formula:

$$\text{Area of a triangle} = \sqrt{d(d - e_1)(d - e_2)(d - e_3)}, \quad (5.3)$$

where  $d = \frac{e_1 + e_2 + e_3}{2}$  is the semiperimeter and  $e_i ; i = 1 : 3$  are the triangle's edges.

To compute the required area, two types of edges are considered: (i) edges connecting two Voronoi vertices and (ii) edges connecting a Voronoi vertex with the intersection point of the sector sideline and a Voronoi edge. Given two vertices, say  $u = (u_1, u_2)$  and  $v = (v_1, v_2)$ , a point  $w = (w_1, w_2)$  lying on the line segment joining them can be determined by:

$$\begin{cases} w_2 = v_2 + \left( \frac{v_2 - u_2}{v_1 - u_1} \right) (w_1 - v_1), \\ d(u, w) + d(w, v) = d(u, v). \end{cases} \quad (5.4)$$

The Voronoi vertices and edges are known from the Voronoi diagram, while the intersection points with the sector sidelines are derived by first formulating the sector sideline equations. Clearly, we get the sector sideline equation when the equality in equation (5.2) holds. Therefore, for a sensor  $s_j$  nominally located at  $(x_j, y_j)$  with a robust position  $t_j = (x'_j, y'_j)$  and the effective sensing range  $r_j$ , the sector sideline equations are given by:

$$\begin{cases} (a_o - x'_j) \cos \theta + (b_o - y'_j) \sin \theta = \sqrt{(a_0 - x'_j)^2 + (b_0 - y'_j)^2} \cos \frac{\theta_s}{2}, \\ d(t_j, p) \leq r_j. \end{cases} \quad (5.5)$$

**Case-3: Voronoi edges intersect sector arc and sidelines** [See  $s_3$  in Figure 5c]. In this scenario, the area is computed similarly to Case 2 by constructing line segments between the sensor's robust position  $t_j$  and the intersection points of the sector boundaries with the Voronoi edges. Given the sensor's robust position  $t_j = (x'_j, y'_j)$ , sensing range  $r_j$ , angle of view  $\theta_s$  and orientation angle  $\theta$ , the area is calculated using equations (5.3-5.5) along with the sector arc equation:

$$\begin{cases} d(t_j, p) = r_j, \\ a_0 \in [r_j \cos(\theta + \frac{\theta_s}{2}) + x'_j, r_j \cos(\theta - \frac{\theta_s}{2}) + x'_j], \\ b_0 \in [r_j \sin(\theta - \frac{\theta_s}{2}) + y'_j, r_j \sin(\theta + \frac{\theta_s}{2}) + y'_j], \end{cases} \quad (5.6)$$

where  $p = (a_0, b_0)$  denotes a point located on the arc boundary of the sensor's coverage sector.

**Case-4: Mixed intersection (cases 2 and 3 combined)** [See  $s_4$  in Figure 5d]. In this case, the sensor's robust position is connected via line segments to all intersection points of the sector arc with Voronoi edges, the sector sideline with Voronoi edges and the Voronoi vertices. The required area  $A_j$  is then determined using equations (5.3-5.6).

After computing the desired coverage area for all four cases, the sensor selects a unit direction vector pointing toward the vertex that provides the maximum coverage. This vector is chosen as the primary optimal orientation direction.

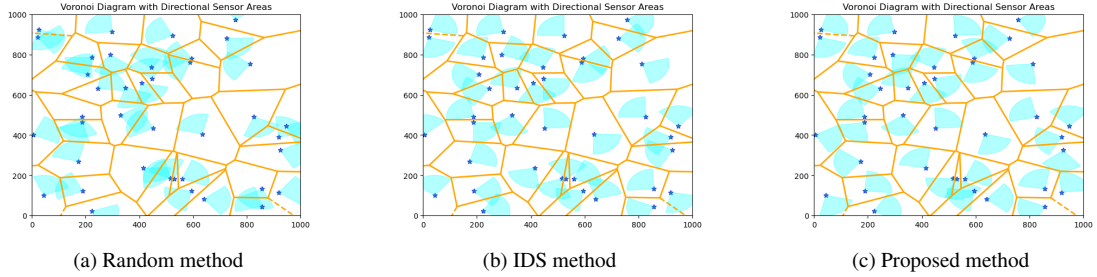


Figure 7: Comparison of sensor orientation strategies: (a) Random method with arbitrary orientations, (b) IDS method optimizing direction iteratively and (c) Robust method, accounting for uncertainty to maximize coverage

### 5.3. Collaborative Directional Adjustment

After each sensor determines its localized optimal orientation, an inter-cell coordination step minimizes sensing redundancy. This involves evaluating neighboring sensors' coverage within the same Voronoi partition and adjusting orientations based on the degree of overlap. The objective is to maximize coverage within each Voronoi cell while avoiding unnecessary redundancy.

For  $i, j \in \{1, 2, \dots, n\}$ , consider two neighboring sensors  $s_i$  and  $s_j$  with robust locations  $t_i$  and  $t_j$ , robust feasibility radii  $\rho(s_i)$  and  $\rho(s_j)$ , and effective sensing radii  $r_i$  and  $r_j$ , respectively. Overlap is checked only if  $d(t_i, t_j) \leq r_i + r_j$ . For simplicity, we assume all sensors share the same sensing radius  $r_s$ , though the approach remains applicable to heterogeneous settings. If both sensors select the same vertex as their localized optimal orientation and  $d(t_i, t_j) \leq r_i + r_j$ , then overlap is inevitable.

When overlap is detected, one sensor reorients toward an uncovered region, prioritizing areas with higher coverage density. The sensor covering the smaller area shifts to the next-best coverage vertex and repeats the process while checking for conflicts with other sensors. The resulting overlap can fall into one of three types, as illustrated in Figure 6, with preferences ordered as (6a), (6b) and (6c), corresponding to decreasing levels of overlap.

### 5.4. Perimeter Coverage Refinement

To reduce coverage wastage near the network boundary perimeter, sensors adjust orientation to limit outward projection and enhance internal coverage. If a sensor is within a threshold  $\epsilon$  of the boundary, vertices within  $\epsilon$  of the vertical or horizontal edges are excluded from its orientation choices. Voronoi–boundary intersection points, treated as vertices, are also omitted. This improves overall field efficiency by focusing boundary sensors inward.

### 5.5. Performance Evaluation and Stopping Criterion

If all vertex options are exhausted without resolving overlap during collaborative directional adjustment, the sensor is assigned the orientation with minimal overlap—energy conservation via deactivation is not considered in this study. We evaluate effectiveness by computing the total sensing area,

$$A(S) = \sum_{j=1}^m A_j,$$

where  $A_j$  is the effective region covered by sensor  $s_j$ ;  $j = 1 : m$ . Performance is further assessed using Voronoi diagrams across deployment scenarios and varying  $\theta_s$  with results visualized through diagrams of initial vs. optimized orientations (see Figure 7), sensor-to-coverage comparison tables and coverage improvement graphs. The algorithm stops when no two sensors share a vertex or all alternative options for overlapping sensors are exhausted.

## 6. Experimental Analysis

In this section, we evaluate the performance of our sensor adjustment strategy under real-world deployment deviations.

### 6.1. Algorithm for Coverage Optimization

To improve DSN efficiency, we employ a structured optimization approach based on Voronoi partitioning. Given the challenges of field of view limits, misalignment and deployment variability, our method iteratively adjusts sensor orientations to maximize the monitored area. Each sensor is aligned to a Voronoi vertex, yielding the greatest coverage gain, promoting an optimal sensing distribution.

The algorithm refines sensor placements by exploring alternative orientations and resolving overlapping coverage. It includes an adaptive mechanism that dynamically adjusts sensor directions, countering deployment inaccuracies and enhancing overall coverage. Detailed steps are provided in Algorithm 1.

---

#### Algorithm 1 Collaborative Voronoi-based sensor orientation optimization

---

**Require:** Initial sensor positions  $S = \{s_1, s_2, \dots, s_m\}$ , corresponding orientations, movement constraints  $\rho$ , sensor radius  $r_s$

**Ensure:** Optimized sensor orientation and positioning to maximize coverage under uncertainty

- 1: **Initialize:** Define sensor positions  $S$ , orientations and Voronoi regions
- 2: Compute initial Voronoi diagram for the given sensor positions
- 3: **Step 1: Perimeter coverage refinement**
- 4: **for** each sensor  $s_i \in S$  **do**
- 5:     Identify Voronoi vertices of  $s_i$
- 6:     Filter vertices that lie within boundary constraints  $[\epsilon, R - \epsilon]$
- 7:     Update valid vertex set for each sensor
- 8: **end for**
- 9: **Step 2: Localized orientation optimization**
- 10: **for** each sensor  $s_i \in S$  **do**
- 11:     Compute the area of each possible orientation using Voronoi partitioning
- 12:     Choose orientation maximizing the Voronoi cell area at the worst case location
- 13:     Update sensor orientation
- 14: **end for**
- 15: **Step 3: Collaborative directional adjustment**
- 16: **repeat**
- 17:     **for** each pair of sensors  $(s_i, s_j)$  where  $s_i$  and  $s_j$  share the same vertex **do**
- 18:         Compute Euclidean distance  $d_{ij}$  between  $s_i$  and  $s_j$
- 19:         **if**  $d_{ij} < \rho_i + \rho_j + 2r_s$  **then**
- 20:             Compute coverage area  $A_i, A_j$
- 21:             Sensor with lower coverage reorients to next best available vertex
- 22:         **end if**
- 23:     **end for**
- 24: **until** All sensors have unique or exhausted orientations
- 25: Compute final Voronoi diagram and compare coverage improvements
- 26: Generate performance metrics and analyze sensor placement effectiveness

---

### 6.2. Experimental Setup

To evaluate our approach, we compare different sensor deployment strategies under uncertainty, using three orientation methods: **Random**, where sensors are oriented arbitrarily; **IDS**, as described in [26]; and our **Proposed method**, which optimizes orientations for maximum coverage under location uncertainty. Experiments are conducted across three deployment scenarios: **Nominal position**, where sensors are placed at ideal positions without considering uncertainty; **Best robust position**, where sensors are optimally positioned for robust feasibility; and **Worst position**, where sensors are placed in the least favorable yet feasible locations.

### 6.3. Performance Metrics and Experimental Results

To evaluate the effectiveness of our approach, we conduct simulations across various network configurations, systematically adjusting key parameters such as the number of deployed sensors  $m$ , angle of view  $\theta$ , sensing

radius  $r_s$  and RRF range  $\rho$ . Performance is measured by analyzing the overall sensing coverage ratio under these conditions. Simulations are carried out in a rectangular region  $R$  of  $(1000 \times 1000)$  square units, with the RRF  $\rho_s$  first computed using Theorem 3.1 and constrained within practical RRF limits. Optimized sensor orientations under uncertainty are then obtained using Algorithm 1 and benchmarked against random and IDS-based orientation strategies. Each configuration is simulated for 500 iterations and the average results are reported to ensure a reliable and robust evaluation. All simulations are implemented in Python 3.12 on a standard computing platform. The tables below present the impact of these parameters on coverage efficiency and robustness. We consider three different sensor positions within its uncertainty set: nominal position (Case I), best robust position (Case II) and worst position (Case III), as detailed in Section 6.2.

**Impact of varying angle of view ( $\theta$ ):** Table 1 presents the results obtained by varying the angle of view  $\theta$  while keeping other parameters constant:  $r_s = 100$ ,  $m = 40$  and  $50 \leq \rho \leq 150$ . This analysis highlights the effect of sensor orientation range on overall coverage performance and robustness.

Table 1: Impact of varying angle of view  $\theta$  on coverage using different deployment strategies (rounded off to nearest integral values).

Deployment strategy	$\theta = 30^\circ$	$\theta = 60^\circ$	$\theta = 90^\circ$	$\theta = 180^\circ$	$\theta = 360^\circ$
<b>Randomly: Case I</b>	91683	174698	249855	439234	682367
<b>IDS: Case I</b>	103095	201701	294041	514600	682367
<b>Our: Case I</b>	102282	198093	285049	498955	682367
<b>Randomly: Case II</b>	86142	161244	227017	381271	553350
<b>IDS: Case II</b>	99792	191454	269011	418503	553350
<b>Our: Case II</b>	100891	191099	265638	402780	553350
<b>Randomly: Case III</b>	84137	161251	231145	412348	663142
<b>IDS: Case III</b>	88480	170534	247504	459801	696195
<b>Our: Case III</b>	91003	171431	244297	451819	809095

**Impact of varying sensing radius ( $r_s$ ):** Table 2 presents the results for different values of sensing radius  $r_s$  and other parameters constant:  $\theta = 90^\circ$ ,  $m = 40$  and  $50 \leq \rho \leq 150$ . This experiment demonstrates how changes in sensor range influence the sensing coverage and system robustness.

Table 2: Impact of varying sensing radius ( $r_s$ ) on deployment strategies.

Deployment strategy	$r_s = 50$	$r_s = 100$	$r_s = 200$	$r_s = 300$
<b>Randomly: Case I</b>	72557	249855	645845	869438
<b>IDS: Case I</b>	78170	294041	686663	876569
<b>Our: Case I</b>	77397	285049	665401	851696
<b>Randomly: Case II</b>	65204	227017	612245	853963
<b>IDS: Case II</b>	68490	269011	764764	937304
<b>Our: Case II</b>	68697	265638	769062	935614
<b>Randomly: Case III</b>	66872	231145	610350	840459
<b>IDS: Case III</b>	73106	247504	580221	834716
<b>Our: Case III</b>	75573	244297	545463	801989

**Impact of varying number of sensors ( $m$ ):** Table 3 examines how the number of deployed sensors affects coverage. Results are for different values of number of sensors  $m$  while other parameters as constant:  $\theta = 90^\circ$ ,  $r_s = 100$  and  $50 \leq \rho \leq 150$ . Increasing the number of sensors can enhance coverage but may also introduce computational challenges.

**Impact of varying radius of robust feasibility:** Table 4 presents the effect of varying the lower ( $\rho_l$ ) and upper ( $\rho_u$ ) bounds of RRF on deployment performance while keeping other parameters constant:  $\theta = 90^\circ$ ,  $r_s = 100$  and  $m = 40$ . This analysis assesses trade-offs between robustness and practical feasibility constraints.

Table 3: Impact of varying number of sensors ( $m$ ) on deployment strategies.

Deployment strategy	$m = 10$	$m = 40$	$m = 60$	$m = 100$
<b>Randomly: Case I</b>	69746	249855	350253	510154
<b>IDS: Case I</b>	77965	294041	409403	568134
<b>Our: Case I</b>	77196	285049	394868	546267
<b>Randomly: Case II</b>	60925	227017	320653	473685
<b>IDS: Case II</b>	71166	269011	378147	549501
<b>Our: Case II</b>	72648	265638	371805	543131
<b>Randomly: Case III</b>	61293	231145	329134	484285
<b>IDS: Case III</b>	74071	247504	320669	436887
<b>Our: Case III</b>	75773	244297	305051	394289

Table 4: Impact of varying radius of robust feasibility on deployment strategies.

Deployment Strategy	$10 \leq \rho \leq 50$	$50 \leq \rho \leq 150$	$200 \leq \rho \leq 500$
<b>Randomly: Case I</b>	249955	249855	248871
<b>IDS: Case I</b>	293648	294041	293506
<b>Our: Case I</b>	288143	285049	255845
<b>Randomly: Case II</b>	233368	227017	221227
<b>IDS: Case II</b>	292848	269011	217123
<b>Our: Case II</b>	291089	265638	224555
<b>Randomly: Case III</b>	237559	231145	192308
<b>IDS: Case III</b>	270802	247504	199356
<b>Our: Case III</b>	269197	244297	178985

#### 6.4. Comparative Analysis

Figure 8 compares area coverage for different sensor orientation strategies, including random, IDS, and the proposed method, across varied deployment scenarios. We use 40 sensors with a sensing radius of 100 units, a sensing angle of 60 degrees, and robust feasibility radii between 50 and 150. The boundary proximity threshold is set to  $r_s/3$ . Subfigure 8a shows the best case with optimal placement and maximum coverage, Subfigure 8b presents the exact case under nominal conditions, and Subfigure 8c depicts the worst case with misalignment and uncertainty. Although the proposed method may slightly reduce peak coverage, it offers improved robustness and reliability under uncertainty. The results show that nominal deployment offers the highest theoretical coverage but lacks robustness under positional uncertainty. Best robust deployment achieves high coverage with only a slight loss in optimality, while worst robust deployment, though feasible, suffers significant coverage loss due to poor positioning. By incorporating RRF into sensor placement, our approach balances robustness and coverage, ensuring reliable performance in uncertain environments with minimal optimality trade-off.

### 7. Conclusions and Future Scopes

Our robust deployment strategy mitigates uncertainty, ensuring a stable, practical solution for real-world sensor networks. Combining Voronoi-based placement with local and inter-cell orientation adjustments, the algorithm optimizes coverage while maintaining resilience to deployment deviations. The integration of RRF further enhances tolerance to misplacements and environmental uncertainty. Despite a slight coverage trade-off, the improved robustness offers a compelling alternative to traditional methods.

For future work, we suggest extending this framework to accommodate different sensor types and incorporating machine learning techniques for predictive coverage adjustments. Additionally, our approach can be adapted for multi-terrain environments by introducing weighted path distances and region-specific feasibility metrics, enabling deployment in complex landscapes with varying terrain constraints. These extensions would further enhance the applicability and effectiveness of the proposed method in diverse real-world scenarios.

Table 5: Comparison of different deployment strategies.

Deployment strategy	Coverage area	Robustness	Computational cost
Random deployment	Lowest	Low	Low
IDS deployment	Slightly higher	Moderate	Moderate
Robust deployment	Moderate	Highest	Slightly higher

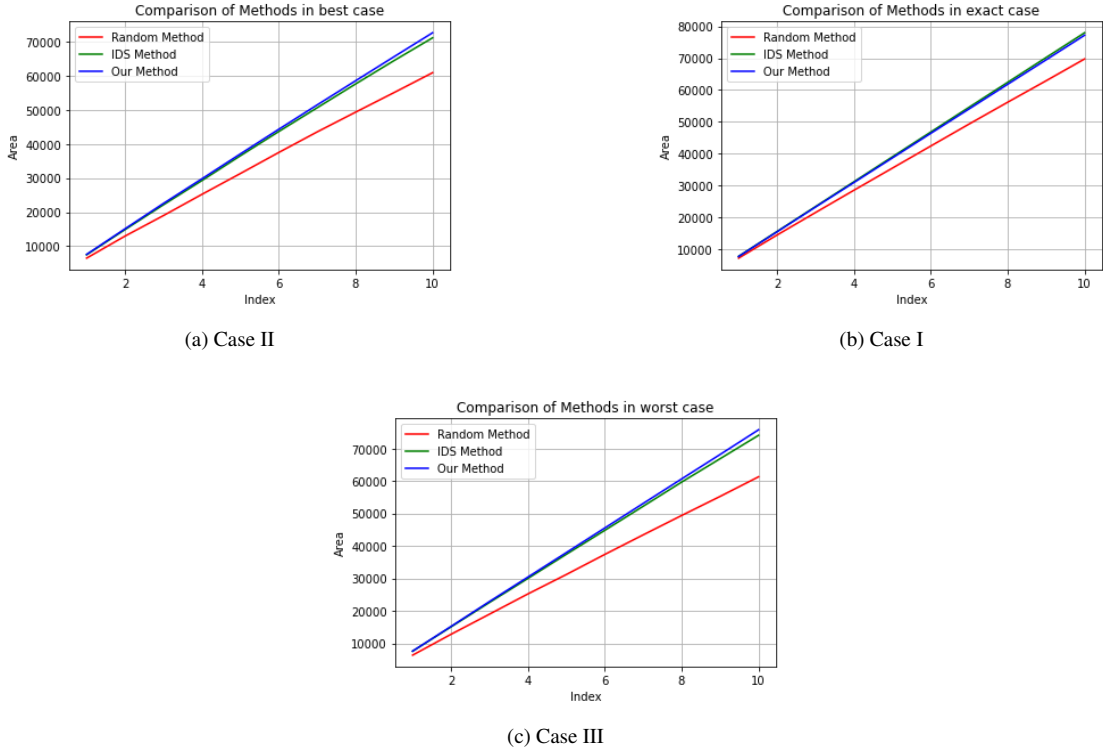


Figure 8: Area coverage comparison under different orientation strategies: (a) Best, (b) Exact, (c) Worst case—for random, IDS and proposed methods

## References

- [1] Ben-Tal, A., El Ghaoui, L., Nemirovski, A.: Robust Optimization. Princeton University Press, Princeton (2009)
- [2] Ben-Tal, A., den Hertog, D., Vial, J.-P.: Deriving robust counterparts of nonlinear uncertain inequalities. *Math. Program. Ser. A* **149**(1-2), 265-299 (2015)
- [3] Ben-Tal, A., Goryashko, A., Guslitzer, E., Nemirovski, A.: Adjustable robust solutions of uncertain linear programs. *Math. Program.* **99**(2), 351-376 (2004)
- [4] Ben-Tal, A., Nemirovski, A.: Robust solutions of uncertain linear programs. *Oper. Res. Lett.* **25**(1), 1-13 (1999)
- [5] Ben-Tal, A., Nemirovski, A.: Robust solutions of linear programming problems contaminated with uncertain data. *Math. Program.* **88**, 411-424 (2000)
- [6] Ben-Tal, A., Nemirovski, A.: Lectures on Modern Convex Optimization—Analysis, Algorithms and Engineering Applications. SIAM, Philadelphia (2001)
- [7] Ben-Tal, A., Nemirovski, A., Roos, C.: Robust solutions of uncertain quadratic and conic-quadratic problems. *SIAM J. Optim.* **13**(2), 535-560 (2002)
- [8] Boyd, S., Vandenberghe, L.: Convex Optimization. Cambridge University Press, Cambridge (2004)

[9] Chen, J., Li, J., Li, X., Lv, Y., Yao, J.C.: Radius of robust feasibility of system of convex inequalities with uncertain data. *J. Optim. Theory Appl.* **184**(2), 384-399 (2020)

[10] Chuong, T.D., Jeyakumar, V.: An exact formula for radius of robust feasibility of uncertain linear programs. *J. Optim. Theory Appl.* **173**(1), 203-226 (2017)

[11] Gabrel, V., Murat, C., Thiele, A.: Recent advances in robust optimization: An overview. *European J. Oper. Res.* **235**(3), 471-483 (2014)

[12] Ghaoui, L.E., Oustry, F., Lebret, H.: Robust solutions to uncertain semidefinite programs. *SIAM J. Optim.* **9**(1), 33-52 (1999)

[13] Goberna, M.A., Jeyakumar, V., Li, G., Linh, N.: Radius of robust feasibility formulas for classes of convex programs with uncertain polynomial constraints. *Oper. Res. Lett.* **44**(1), 67-73 (2016)

[14] Goberna, M.A., Jeyakumar, V., Li, G., Vicente-Pérez, J.: Robust solutions of multiobjective linear semi-infinite programs under constraint data uncertainty. *SIAM J. Optim.* **24**(3), 1402-1419 (2014)

[15] Goberna, M.A., Jeyakumar, V., Li, G., Vicente-Pérez, J.: Robust solutions to multi-objective linear programs with uncertain data. *European J. Oper. Res.* **242**(3), 730-743 (2015)

[16] Goberna, M.A., Jeyakumar, V., Li, G., Vicente-Pérez, J.: The radius of robust feasibility of uncertain mathematical programs: A Survey and Recent Developments. *European J. Oper. Res.* **296**(3), 749-763 (2022)

[17] Goberna, M.A., López-Cerdá, M.A.: *Linear Semi-Infinite Optimization*. Wiley, Chichester (1998)

[18] Kouvelis, P., Yu, G.: *Robust Discrete Optimization and Its Applications*. Springer, Berlin (2013)

[19] Leyffer, S., Menickelly, M., Munson, T., Vanaret, C., Wild, S.M.: A survey of nonlinear robust optimization. *INFOR Inf. Syst. Oper. Res.* **58**(2), 342-373 (2020)

[20] Li, X.B., Wang, Q.L.: A note on the radius of robust feasibility for uncertain convex programs. *Filomat* **32**(19), 6809-6818 (2018)

[21] Li, Z., Ding, R., Floudas, C. A.: A comparative theoretical and computational study on robust counterpart optimization: I. Robust linear optimization and robust mixed integer linear optimization. *Industrial & Engineering Chemistry Research, ACS Publications*, **50**(18), 10567-10603 (2011)

[22] Ridolfi, A.B., Vera de Serio, V.N.: A Radius of Robust Feasibility for Uncertain Farthest Voronoi Cells. *Set-Valued Var. Anal.* **31**(1) (2023)

[23] Sahinidis, N.V.: Mixed-integer nonlinear programming. *Optim. Eng.* **20**(2), 301-306 (2019)

[24] Schirotzek, W.: *Nonsmooth analysis*, Universitext Series. Springer Science & Business Media, Springer, Berlin (2007)

[25] Soyster, A.L.: Convex programming with set-inclusive constraints and applications to inexact linear programming. *Oper. Res.* **21**(5), 1154-1157 (1973)

[26] Sung, T. W., Yang, C. S.: Voronoi-based coverage improvement approach for wireless directional sensor networks. *J. Netw. Comput. Appl.* **39**, 202-213 (2014)

[27] Ye, W., Ordonez, F.: Robust optimization models for energy-limited wireless sensor networks under distance uncertainty. *IEEE transactions on wireless communications, IEEE*, **7**(6), 2161-2169 (2008)

[28] Yuan, Y., Li, Z., Huang, B.: Nonlinear robust optimization for process design. *AIChE* **64**(2), 481-494 (2018)

- [29] Zhang, Q., Grossmann, I. E., Lima, R. M.: On the relation between flexibility analysis and robust optimization for linear systems. *AIChE*. **62**(9), 3109-3123 (2016)
- [30] Zhang, Y.: General robust-optimization formulation for nonlinear programming. *J. Optim. Theory Appl.* **132**(1), 111-124 (2007)